ELSEVIER

Journal of Power Sources 64 (1997) 117–122

JOURNAL OF POWER SOURCES

Structural and morphological study of damage in lead/acid batteries during cycling and floating tests

C. Brissaud [a,b,*], G. Reumont [a], J.P. Smaha [b], J. Foct [a]

[a] *Laboratoire de Métallurgie Physique, CNRS URA 234, Université de Lille I, 59655 Villeneuve d'Ascq Cedex, France*

[b] *OLDHAM France S.A., Service Technique, 62033 Arras Cedex, France*

Abstract

Premature capacity loss is a severe problem observed in lead/acid batteries; it has been localised at the grid/positive active material interface (PAM) and in the PAM. In order to understand these phenomena, cycled batteries with Pb–Sb–Sn and Pb–Ca–Sn positive grid alloys were studied and compared with floated batteries with Pb–Ca–Sn positive grid alloys. The evolution of the crystallographic and morphological structure of the PAM and of the grid/PAM interface during the tests were investigated. Formation of isolated agglomerates of PAM by the phenomena assimilated to sintering was found to be the reason of the failure of cycled batteries, whereas the intergranular corrosion of the grid initiated the floated batteries' end of life. The results and mechanisms of these phenomena are presented.

Keywords: Lead/acid batteries; Cycling tests; Floating tests; Premature capacity loss; Positive active material

1. Introduction

Premature capacity loss (PCL) is a severe problem for lead/acid batteries and has been the subject of many studies. Batteries in which PCL phenomena occur, show a life time which is reduced compared with the expected life. An early and rapid decrease of capacity occurs long before the natural ageing of the battery (active material shedding and grid corrosion which limit battery performance). PCL is particularly severe in batteries with positive plates that use antimony-free or low-antimony grid alloys.

In this paper, PCL phenomena have been studied on batteries with Pb–Ca–Sn and Pb–Sb–Sn alloys at the positive grid. Cycled batteries with Pb–Sb–Sn alloys at the positive grid have been used as a reference and compared with cycled and floated batteries with Pb–Ca–Sn alloys positive grids.

Positive active material (PAM) and grid/PAM interface analyses allow interpretation of the phenomena which occur in the positive plate.

2. Experimental

Table 1 provides a summary of the different groups of 2 V valve-regulated lead/acid (VRLA) cells with absorption glass mat (AGM) construction which have been tested.

Table 1
Composition of batteries tested

Positive grid alloy	Test
Pb–Sb–Sn	Cycling
Pb–Ca–Sn	Cycling
Pb–Ca–Sn	Floating

Each cell was composed of twelve positive plates, thirteen negative plates and twelve glass fiber separators. The plate dimensions were 136 mm × 136 mm × 2.5 mm. After formation, the cells contained a 1.29 sp. gr. sulfuric acid solution. All the plates had the same curing and all the batteries, the same assembly and active material formation procedure. The composition of the PAM is given in Fig. 1. The 5 h capacity (C_5) of the batteries was 120 Ah.

The cycling test consisted of a discharge during 3 h at 30A constant current ($C_{5/4}$) followed by an *IU* charge procedure which consists of a charge at a constant current ($C_{5/5}$) limited by a voltage of 2.35 V per cell. Capacity was measured every hundred cycles at the $C_{5/5}$ rate until the tension reaches 1.7 V per cell. The test was ended when the capacity of the cell was 25% lower than the initial one.

The second test realised on the third group of batteries was a 2.27 V floating test at a temperature of 55 °C. Every 40 days, performance was checked at a rate of $C_{20/0.67}$ at room

* Corresponding author.

0378-7753/97/$17.00 © 1997 Elsevier Science S.A. All rights reserved
PII S0378-7753(96)02511-6

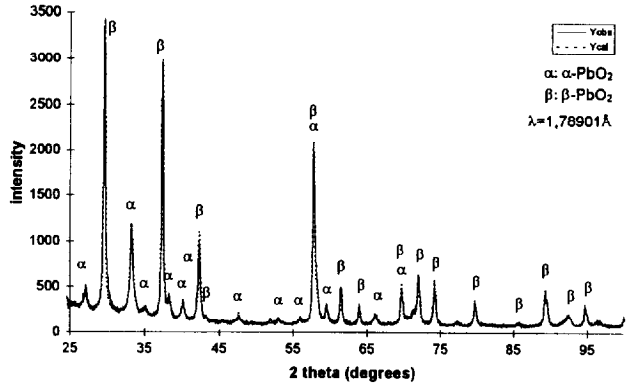

Fig. 1. Rietveld profile refinement of a PAM X-ray diffraction pattern (comparaison between calculated and observed intensity).

temperature. The test was stopped when the remaining capacity was less than the 80% of the initial $C_{20/0.67}$ capacity at room temperature. At different stages of the tests, some cells were taken off and dismantled. The central positive plates were washed and dried. Each stage was investigated using different structural and morphological methods.

X-ray diffraction (XRD) analyses of PAM were performed with a Siemens D500 diffractometer equipped with a cobalt anode. Samples were prepared from pellets taken off from the positive plate and which were ground to powder. Crystallographic phase identification was performed using the powder diffraction files (PDF) files [1]: α-PbO_2 [37-517], β-PbO_2 [41-1492] and $PbSO_4$ [36-1461] files. The Rietveld method [2] based on the background, atomic positions, cell parameters, preferentiel orientation refinements, was used to quantify the different phases detected on each spectrum.

The microscopic observations were performed with either an optical microscope and/or a Philips 525M scanning electron microscope (SEM). Microprobe wavelength dispersion spectroscopy (WDS) analysis were carried out with a Camebax system. The samples were taken off with a diamond–thread-saw from epoxy resin coated positive plates and polished up to 3 μm.

Different stages of life were analysed: just after formation, after 100 and 200 cycles or 120 days of floating and at the end of life.

3. Results

3.1. PAM analysis

3.1.1. Crystalline phase analysis of the PAM

The qualitative and quantitative crystalline phase analysis were tested at different stages of the life of the batteries and at different places in the plates: at the top, middle and bottom. The crystalline phases found in the PAM are α-PbO_2 (orthorhombic system), β-PbO_2 (tetragonal system) and sometimes $PbSO_4$ (othorhombic system). After the identification of the phases, a refinement of the spectrum with the Rietveld

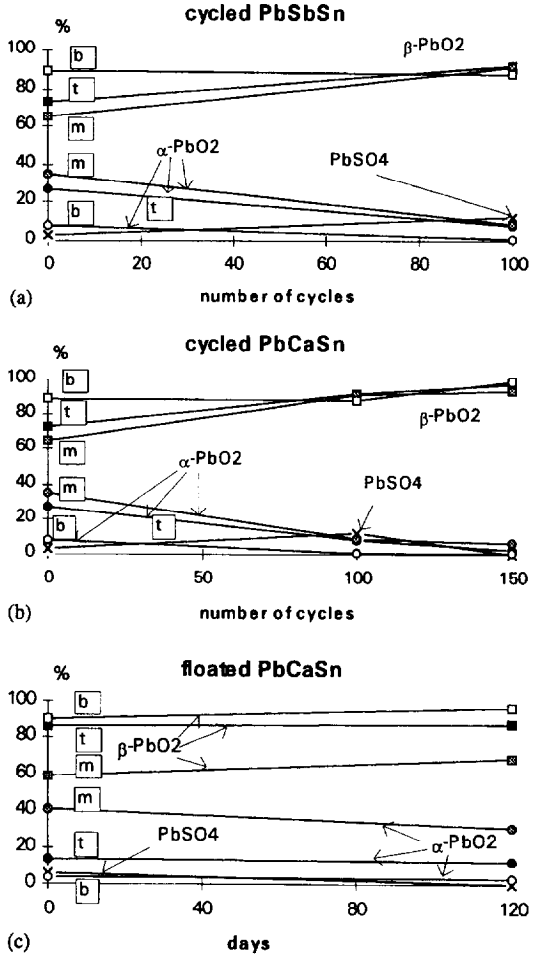

Fig. 2. Evolution of the crystalline phase PAM composition during life of the battery: (b) bottom; (t) top, and (m) middle.

method is realised (Fig. 1). Fig. 2(a)–(c) illustrates the XRD quantitative analysis results.

Fig. 2 shows that the crystalline phase composition of the PAM versus number of cycles or number of days of floating depends only on the initial composition of the PAM and not on the positive grid alloy. The evolution of this composition reveals that α-PbO_2 tends to disappear. On the other hand, the composition depends on the place in the plate where the PAM is taken off. The middle of the plate contains more α-PbO_2 than the top. The bottom of the plate has the lowest quantity of α-PbO_2. Sometimes, some $PbSO_4$ is observed at the bottom part of the plate.

3.1.2. Morphological structure of the PAM

Analyses of the morphological structure of the PAM were carried out at the top and bottom of the plates at different stages of life of the battery.

3.1.2.1. Cycling test

The evolution of the morphology of the PAM for cycled batteries is the same whatever the positive grid alloy is; it is represented by Fig. 3. After the formation of active material, the PAM is composed of a network of PbO_2 particles which are well connected to each other and to the grid/corrosion

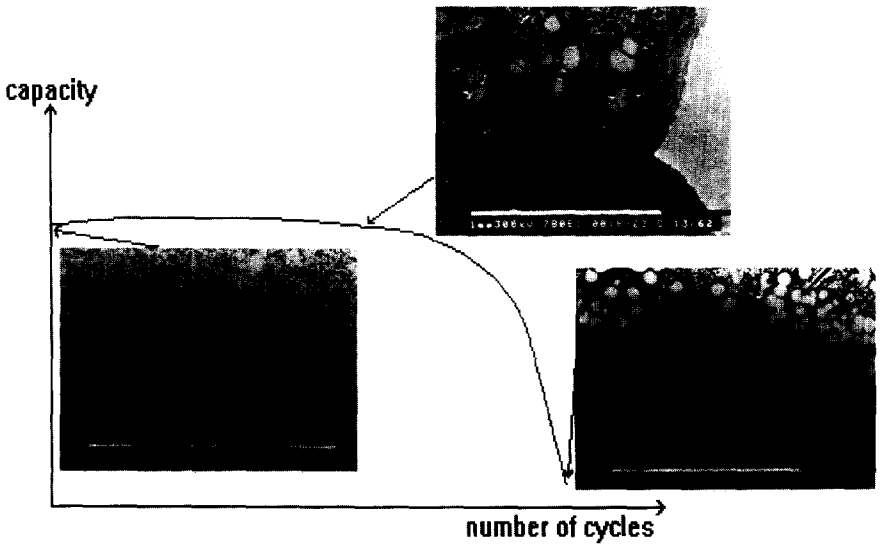

Fig. 3. Morphological PAM evolution vs. ageing of a cycled battery.

layer interface as well. After a few cycles, aggregates of PAM are found near the wire and near the external surface of the plate. These PAM islands are still connected to the rest of the active material. During ageing of the battery, the quantity of PAM aggregates increases. They become more and more isolated from the rest of the PAM. At the end of life, the presence of a lot of isolated PAM aggregates is observed.

This evolution is the same for all the cycled batteries. However, the kinetics of these phenomena depend on the positive grid alloy composition: the kinetics are slower in Pb–Sb–Sn batteries than those observed in Pb–Ca–Sn batteries.

3.1.2.2. Floating test

After the formation of the active material of the floated batteries, the PAM is composed of a dense network of PbO_2 particles. These particles are often found in an island structure connected to each other by the PAM with a lamellar structure (Fig. 4). The morphological aspect of the PAM is always the same during the test.

Fig. 4. PAM microstructure of a floated battery which consists of agglomerates bonded to each other by thin strips of PAM (lamellar structure).

3.2. Grid/PAM interface analysis

The interface between the positive grid and PAM is composed of a corrosion layer which is formed during curing and the formation of active material. Then, the corrosion is a monolayer of PbO_2 of which the thickness depends on the positive grid alloy: the thickness of the corrosion layer for a Pb–Sb–Sn and for a Pb–Ca–Sn positive grid alloy is 24 and 15 μm, respectively.

At the end of life, the structure of the grid/PAM interface depends on the positive grid alloy and on the test (floating or cycling) which has been executed.

For cycled batteries with Pb–Sb–Sn positive grid alloys [3], the thickness of the corrosion layer is about 450 to 500 μm and presents a two-layer morphology (Fig. 5). The internal sub-layer (adjacent to the grid wire) is dense, slightly cracked, and is 150 μm thick. The cracks are parallel to the

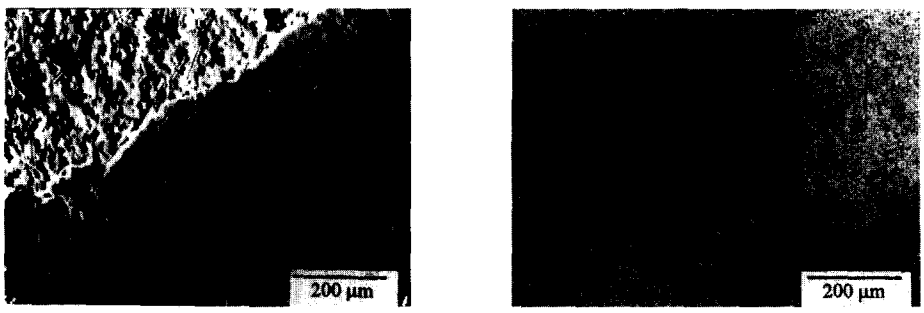

Fig. 5. Cycled Pb–Sb–Sn battery: SE and oxygen X-ray images.

Fig. 6. Cycled Pb–Ca–Sn battery: SE and oxygen X-ray images.

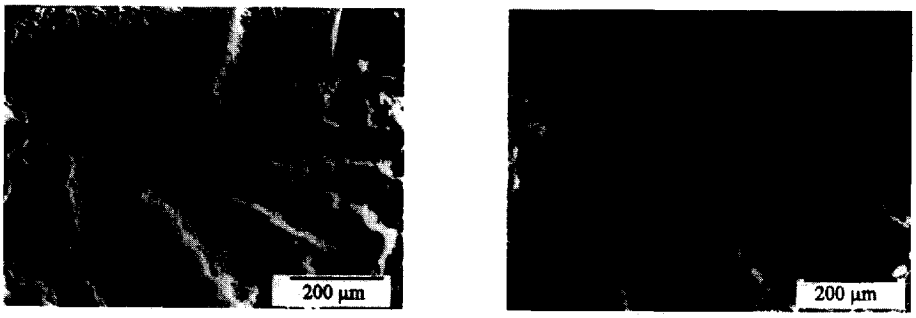

Fig. 7. Floated Pb–Ca–Sn battery: SE and oxygen X-ray images.

external surface of the wire. This sub-layer is composed of PbO. The external sublayer (adjacent to the PAM) is very cracked and has a thickness of 300 µm. The cracks are parallel and perpendicular to the external surface of the wire. It is composed of PbO_2. A de-cohesion between the PAM and the corrosion layer can be noted.

For cycled batteries with a Pb–Ca–Sn positive grid alloy, the interface grid/PAM is a dense monolayer of PbO_2 (Fig. 6). It is about 40 µm thick. There is a good cohesion between the PAM and the corrosion layer.

The grid/PAM interface of the floated batteries with a Pb–Ca–Sn grid alloy is very different because the corrosion of the grid is intergranular. At the end of life, the wires are strongly corroded. The corrosion product is PbO_2 (Fig. 7).

4. Discussion

4.1. Crystallographic structural evolution of the PAM

During cycling, the ratio β-PbO_2/α-PbO_2 increases. This confirms the transformation of α-PbO_2 to β-PbO_2 via $PbSO_4$. During charge, a part of $PbSO_4$ produced from α-PbO_2 is changed into β-PbO_2 [4,5]

$$\left.\begin{matrix} a\times\alpha\text{-}PbO_2 \\ b\times\beta\text{-}PbO_2 \end{matrix}\right\} \overset{\text{discharge}}{\rightarrow} (a+b)PbSO_4 \overset{\text{charge}}{\rightarrow} \left\{\begin{matrix} (a-x)\times\alpha\text{-}PbO_2 \\ (b+x)\times\beta\text{-}PbO_2 \end{matrix}\right. \quad (1)$$

where a and b are the quantity of α- and β-PbO_2 before discharge, and x the quantity of α-PbO_2 which is converted into β-PbO_2 after the charge.

This plays an important part in the behaviour of the PAM. β-PbO_2 is known to give a good capacity and α-PbO_2 to improve the mechanical characteristics of the PAM. During cycling, the amount of α-PbO_2 decreases and becomes negligible at the end of life. The PAM mechanical integrity loss appears therefore to result from this reducing quantity of α-PbO_2.

Meanwhile, the fact that the composition of the PAM of the Pb–Sb–Sn batteries cycled 200 times is quite similar to that of cycled Pb–Ca–Sn batteries at the end of life seems to demonstrate that, in this case, the end of life is not due to the absence of α-PbO_2 but more likely to the morphological structure of the PAM.

4.2. Morphological evolution of the PAM

The ageing of the PAM of a cycled battery is characterized by the development of agglomerates of PAM which are isolated from the rest of the PAM at the end of life. This phenomon is assimilated to sintering.

Sintering [6,7] is a sphere-assembling mechanism which occurs in a solid state. The spherical particles bond each other and create a jonction zone called 'neck zone'. During sintering, the system tends to minimize the superficial energy through different mechanisms: viscous flow, evaporation/condensation and diffusion (surface, volume or grain boundary). Each mechanism has its own law of growth. The sintered spheres are characterized by the radius of the spheres and of the neck zone. Measurements of these physical parameters during the cycling test show that a volume diffusion mechanism takes place during sintering.

The influence on the positive plate capacity of such a phenomenon has been studied by Winsel and co-workers [8,9]. They demonstrate that the electric resistance of the PAM depends on its physical structure [10]: the smaller is the neck

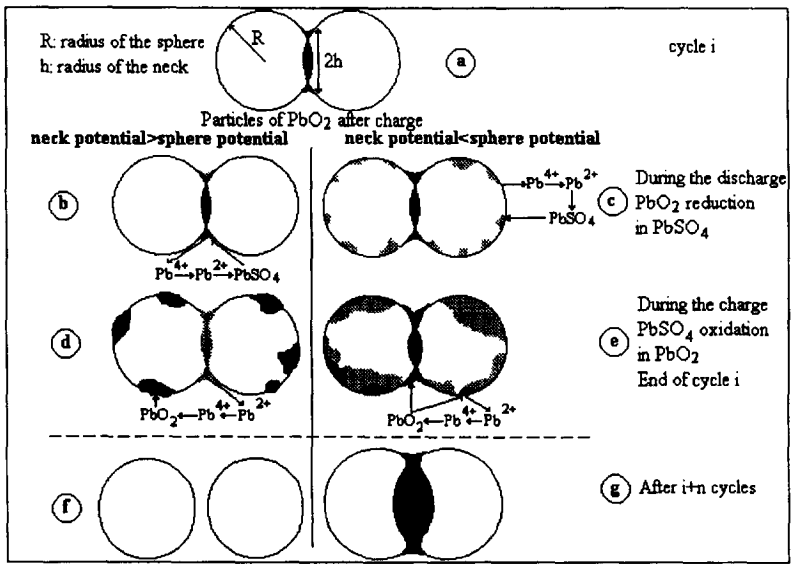

Fig. 8. Mechanisms of (b), (d), (f) isolation of PAM particles, or (c), (e), (g) formation of aggregates of PAM particles during cycling.

zone between two spheres of PbO_2, the higher is the electric resistance and the smaller is the capacity. On a thermodynamical point of view, the difference of chemical potential $\Delta\mu$ between the neck zone and the spheres is associated to an oxygen deviation δ in the stoichiometric composition of the lead dioxide in each zone: $PbO_{2-\delta}$. The chemical potential $\Delta\mu$ depends also on the structural parameters of the sintered spheres such as the radius of the neck and the sphere. They assume that the potential of the neck zone is more negative than that of the sphere, which protects the neck from being electrochemically sliced off during passage of a discharge current.

This phenomenon is quite similar to sintering. But as it occurs only during the cycling test, it means that it is not the only mechanism which takes place in the formation of the aggregates of spheres. Modelling the evolution of the PAM presented in Fig. 8 will try to explain the phenomenon during cycling.

During cycling, after charge, the PAM may be assimilated to spherical particles of PbO_2 which are connected to each other by a neck zone (Fig. 8(a)). When discharging [11], PbO_2 is reduced to $PbSO_4$ via the dissolution of PbO_2 into Pb^{4+} ions. These ions are reduced into Pb^{2+} ions and precipitated as $PbSO_4$. If the potential of the neck zone is smaller than that of the sphere, the reduction occurs preferentially on the sphere surface (Fig. 8(c)). In the other case, the reaction takes place in the neck zone (Fig. 8(b)). The main consequence is the precipitation of $PbSO_4$ in the neck zone. During the charge, lead sulfate is oxidized into lead dioxide. If the potential of the neck zone is smaller than that of the sphere, oxidation occurs preferentially in the neck zone. In this case, the radius of the neck zone increases (Fig. 8(e)). In the other case, a part of the Pb^{2+} ions, which are formed from the neck, are oxidized on the sphere (Fig. 8(d)) and so the neck size decreases. After many cycles, if the potential of the neck zone is smaller than that of the sphere, the jonction zone grows and the distance between the centre of the spheres decreases (Fig. 8(g)): aggregates of PAM are created and sintering achieved. If the potential in the neck zone is higher than that of the sphere, the neck zone decreases which involves the separation of the particles (Fig. 8(f)).

In our cycling test, micrographical observations of PAM sintering necessary establish that the chemical potential of the neck zone is smaller than that of the sphere.

The development of the aggregates of spheres due to the increase of the neck zone implies a densification so that, when agglomerates of PbO_2 are created, they are also more and more isolated from each other during cycling. This implies a decrease in capacity, as observed.

Since the formation of isolated agglomerates of PAM is due to the cycles of charge/discharge, it cannot be observed in the floated batteries. This explains the reason of a good network of PAM for the floated batteries at the end of life.

4.3. *Interfacial evolution during cycling*

The different morphologies and compositions of the interface can be explained by the kinetics of the oxidation reactions which take place on the grid/PAM interface or by mechanisms which occur during the storage of a battery.

The oxidation of the lead of the grid during cycling is comprised of three steps [12–15]:

$$Pb \rightarrow \alpha\text{-}PbO \quad (2)$$

$$\alpha\text{-}PbO \rightarrow PbO_x \quad (3)$$

$$PbO_x \rightarrow \alpha\text{-}PbO_2 \quad (4)$$

Kinetics are controlled by oxygen diffusion. It is well known that the slowest reaction imposes its kinetics. If the kinetics of the α-PbO formation are equal to that of α-PbO_2, the corrosion layer will comprise two sublayers: one of α-PbO and another of α-PbO_2, as observed in the case of cycled

Pb–Sb–Sn batteries. If the kinetics of the α-PbO formation are slower than that of α-PbO_2, then the corrosion layer will comprise a layer of α-PbO_2, as shown by cycled Pb–Ca–Sn batteries.

The cycled Pb–Sb–Sn battery on which the analysis were realised, has been stored during four months after its end of life, and before being dismantled.

At the grid/PAM interface, the reaction between the lead of the grid which is oxidized and the lead dioxide of the corrosion layer which is reduced [13], is given by the following equations:

$$Pb + H_2O \rightarrow PbO + 2H^+ + 2e^- \quad (5)$$

$$PbO_2 + 2e^- + 2H^+ \rightarrow PbO + H_2O \quad (6)$$

$$Pb + PbO_2 \rightarrow 2PbO \quad (7)$$

A grid/PAM interface which is comprised by a lead dioxide layer after a cycling test, is converted into a two-layer structure: a PbO sub-layer and a PbO_2 one. This morphology is observed for the cycled Pb–Sb–Sn battery at the end of life after storage. The observations of the interface during cycling and before the end of life of Pb–Sb–Sn batteries show a dense layer of PbO_2. So it can be supposed that the grid/PAM interface of the cycled Pb–Sb–Sn batteries is comprised by a monolayer of lead dioxide. Future observations of cycled Pb–Sb–Sn batteries at the end of life without storage will confirm this assumption.

The grid/PAM interface of cycled batteries (Pb–Ca–Sn and Pb–Sb–Sn) is only composed of lead dioxide.

4.4. Corrosion mechanism during floating

For the floated Pb–Ca–Sn batteries, the corrosion of the grid is intergranular. During discharge of the positive plate, PbO_2 is reduced to $PbSO_4$. During charge, $PbSO_4$ is oxidized to PbO_2. During floating, the transformation of the PAM to PbO_2 is followed by the oxidation of the lead of the grid. The grid lead does not correspond to the most oxidized form, this explains why it reacts during overcharge. The oxidation of the grid is so fast that it appears to be the reason for the failure of the batteries: electric current cannot be collected and during the oxidation, because of the increasing of the molar volume (the molar volume of PbO_2 is higher than that of Pb) the grid loses its shape and connections with the PAM.

5. Conclusions

The grid/PAM interface and the morphological structure of the PAM depend on the positive grid alloy and on the test procedure. The main conclusions of the study are:

(i) For cycled (Pb–Ca–Sn and Pb–Sb–Sn) batteries, the corrosion layer is only comprised of a monolayer of PbO_2. The morphological structure of the PAM is the reason for the end of their life. The PAM is then composed of isolated aggregates of PAM which have been formed by a mechanism assimilated to sintering during the charge/discharge cycles.

(ii) The storage of a cycled battery implies a two-layer structure for the grid/PAM interface (one sub-layer of PbO and another of PbO_2).

(iii) The corrosion of the positive grid for floated Pb–Ca–Sn batteries is intergranular and the corrosion product is PbO_2. The PAM is composed of a network of PbO_2 particles which are well connected together, even at the end of life. Meanwhile, the failure of the floated Pb–Ca–Sn batteries appears to result from the corrosion of the grid which becomes unable to collect the electric current and creates a de-cohesion between PAM and grid which then loses its shape. This contributes to the loss of capacity of such batteries.

References

[1] *JCPDS Files* (Joint Committee on Powder Diffraction Standards Files), International Union of Crystallography, Oxford Scientific Publications, Oxford University Press, London, 1993.
[2] R.A. Young, *The Rietveld Method*, Oxford Science Publications, Londen, 1993.
[3] C. Brissaud, P. Lenain, J.P. Smaha, X. Muneret, G. Reumont and J. Foct, *Sci. Génie Mater.*, *9* (1994) 1358.
[4] K. Harris, R.J. Hill and D.A.J. Rand, *J. Power Sources*, *8* (1982) 175.
[5] K. Harris, R.J. Hill and D.A.J. Rand, *J. Electrochem. Soc.*, *131* (1984) 474.
[6] Y. Adda, J.M. Dupouy, J. Philibert and Y. Quéré, *Elém. Métall. Phys.*, *4* (1987) 990.
[7] J. Philibert, *Atom Movements — Diffusion and Mass Transport in Solids*, Monographies de Physique, Editions de Physique, Les Ulis, france, 1991.
[8] U. Hullmeine, A. Winsel and E. Voss, *J. Power Sources*, *25* (1989) 27.
[9] A. Winsel, E. Voss and U. Hullmeine, *J. Power Sources*, *30* (1990) 209.
[10] A.F. Hollenkamp, *J. Power Sources*, *36* (1991) 567.
[11] A.J. Bard and L.R. Faulkner, *Electrochimie — Principes, Méthodes et Applications*, Masson, Paris, 1983.
[12] B. Culpin, A.F. Hollenkamp and D.A.J. Rand, *J. Power Sources*, *38* (1992) 63.
[13] K.R. Bullock and M.A. Butler, *J. Electrochem. Soc.*, *133* (1986) 1085.
[14] D. Pavlov, *J. Power Sources*, *53* (1995) 9.
[15] D. Pavlov, *J. Power Sources*, 48 (1994) 179.